Characterisation of Radiation Damage in Perovskite Superconductor Yttrium Barium Copper Oxide

S. Pedrazzini[1], M. Danaie[1], G. D. Brittles[1], S. Speller[1], C. R. M. Grovenor[1], P. D. Edmondson[2], M. P. Moody[1], P. A. J. Bagot[1]

[1] *Department of Materials, University of Oxford, Parks Road, OX1 3PH, Oxford, UK.*
[2] *Oak Ridge National Laboratory, 1 Bethel Valley Road, Oak Ridge, TN 37831, Tennessee, USA.*

Abstract

High temperature superconducting materials are currently utilised to generate the magnetic fields required for the confinement of plasma in fusion reactors. The present study aims to assess the microstructural degradation resulting from ion implantation at room temperature with 2 MeV Xe^+ ions to a total fluence of 1 x 10^{16} ions/cm^2 in Yttrium Barium Copper Oxide (YBCO) using high-resolution characterisation techniques. Atom Probe Tomography (APT) and Transmission Electron Microscopy (TEM) analyses were performed and correlated with alterations in superconducting behaviour measured using a Magnetic Properties Measurement System (MPMS). TEM analysis was performed to depth-profile the degree of crystallinity on irradiated samples. The maximum-damage layer was found 800 nm below the sample surface. Ion implantation caused the superconducting temperature to decrease by 10 K and the critical current density to display a 10-fold reduction.

1. Introduction:

High temperature superconductor Yttrium Barium Copper Oxide (YBCO) has been proposed as a candidate material for magnetic confinement of plasma in nuclear fusion reactors due to the advantage it has over Nb_3Sn low temperature superconductor (*1*). HTS tape can be activated at relatively low neutron doses due to the nickel superalloy substrate it is grown on, which can form unstable isotopes through transmutation, such as for example ^{60}Co. Knowledge of the conditions which will cause degradation of the superconducting properties to a level in which they will no longer create confinement is a crucial consideration, which can then be fed into the reactor design so that an adequate level of shielding can be selected. Keeping shielding to the minimum required amount would allow substantial savings in construction and decommissioning costs and reduce environmental impact, while still ensuring that the functional properties of the material will not be lost over the lifetime of the reactor.

It is therefore essential for the assessment of candidate materials to study their electrical and microstructural response to radiation damage. Room temperature ion implantations at low-fluence have been shown to increase the critical current density of YBCO through generation of new pinning sites (*2*). This effect is counterbalanced at higher fluences by damage within the crystal structure and oxygen loss, both of which can arise from radiation damage and reduce the critical current density carried by the superconductor. The exact transition point after which the beneficial effects become detrimental is not well understood and is a key limiting factor in designing the potential lifetime of the superconducting windings (*3*), (*4*).

Previous studies on irradiated YBCO characterised the implanted material, but only at relatively low fluences, up to 1x10^{13} ions/cm^3 (*2*, *5–10*). These studies, available in the scientific literature, on neutron or ion irradiated YBCO focus on the beneficial effects, which include small increases in critical temperature T_c, and comparatively larger increases in critical current density J_c through the generation of new flux pinning sites (*5–9*). A few studies were found in which the transition point in which the effects become detrimental was mapped: Suvorova *et al.* (*2*) irradiated their samples of SuperPower tape with 107 MeV Kr^+ ions varying the fluence between 2x10^{10} and 6x10^{13} ions/cm^2. They found that above a fluence of 8x10^{11} ions/cm^2 both J_c and T_c decreased abruptly, however they only proceeded to characterise the sample in which the superconducting properties were maximised. In another study, Antonova *et al.* (*10*) used SuperPower HTS tape samples, in which the Cu stabilising layer was etched off revealing the Ag overlayer, which was not removed. They irradiated their samples with varying fluences of 167 MeV Xe^+, 107 MeV Kr^+ and 48 MeV Ar^+ ions and found that the critical temperature T_c starts to reduce at fluences $\phi \geq 1x10^{11}$ ions/cm^2 and above 5x10^{12} ions/cm^2 superconductivity is completely absent. They complemented those

measurements with X-ray diffraction, with which they proved that the material was fully amorphous above those fluences. They noted that X-ray peak positions remained unaltered with increasing fluence, only their height decreased. This indicates that no lattice swelling is detected due to ion implantation, only amorphisation.

However, there are two essential aspects which must be addressed by the characterisation procedure: accurate atomic scale quantification of the oxygen stoichiometry and an assessment of the level of amorphisation/crystallinity, both of which can be altered by exposure to radiation and both of which are crucial for superconducting properties. The present study relies on APT as a method which allows the measurement of oxygen stoichiometry (a detailed study of which is available in a previous publication (*11*)), and transmission electron microscopy (TEM) to assess the degree of crystallinity/amorphisation caused by exposure to ion implantation. The two techniques combined allow a comprehensive characterisation of the microstructures, which complemented by use of superconducting quantum interference device (SQUID) magnetometry measurements leads to improved understanding of the degradation of superconducting properties due to ion implantation.

2. Experimental Methods:

Single crystal YBCO samples were produced by the Top Seeded Melt Growth (TSMG) process (*12*) by the Bulk Superconductivity Group at the University of Cambridge. Powders of the required compositions were pressed into a compact pellet, followed by melting peritectic regrowth of the $Y_1Ba_2Cu_3O_{7-\delta}$ phase (Y-123). A chemically stable $GdBa_2Cu_3O_{7-\delta}$ seed was used as a heterogeneous nucleation site for epitaxial growth of a large Y-123 single crystal, containing additional $Y_2Ba_1Cu_1O_5$ phase (Y-211) particles as inclusions. An optimum amount of 20-30% of $Y_2Ba_1Cu_1O_5$ phase is required to produce an optimum microstructure for flux pinning (*12*). Samples were then cut and polished along the <a> axis up to a 1μm diamond finish using ethanol as a lubricant. Samples of 4 mm wide 2G-HTS tape from SuperPower Inc. were also analysed and irradiated both to perform a bulk-tape comparison and for ease of superconductivity measurements. The 1μm thick layer of YBCO, which was delivered with a Cu stabilising layer and Ag overlayer was exposed by etching with ferric chloride and a combination of ammonium hydroxide and hydrogen peroxide respectively. The oxide based buffer layers and Hastelloy substrate on which the YBCO was grown were however not removed, maintaining the structural integrity of the tape. Previous measurements have shown that this chemical etching process does not harm the superconducting properties of the wire (*13*). The samples were cut into 3 mm diameter discs, mounted in standard plastic straws and loaded into the MPMS with the applied field held perpendicular to the surface of the tape.
Ion implantations were performed on bulk and tape samples at the University of Surrey Ion Beam Centre. Room temperature 2 MeV Xe^+ ions were implanted into the sample to a total fluence of $1x10^{16}$ ions/cm^2.
Samples were prepared for APT and TEM analyses using standard lift-out techniques on a Zeiss NVision 40 focussed ion beam (FIB) microscope.
A Cameca LEAP 3000X HR was used for Atom Probe analysis at the University of Oxford. Samples were run in LASER mode, with a pulse frequency of 160 kHz, a temperature of 50 K and laser energy of 0.05nJ (*11*). TEM analysis was performed on a JEOL 2100 microscope equipped with an Oxford Instruments Energy Dispersive X-ray detector (EDX). Crystallinity and amorphisation were shown through the acquisition of selected area diffraction patterns across the ion implanted area.
Superconductivity temperature and critical current density measurements were performed using a Quantum Design SQUID, using the 3mm disc samples of etched SuperPower tape, oriented with the applied field B//<c> axis. Measurements were performed varying the applied field between 0.01 - 6 T and the temperature between 4.2 - 77 K.

3. Results:

4. 1: Microstructural characterisation of the unirradiated samples

The TSMG process produced a homogeneous microstructure consisting of discrete Y-211 particles <5μm in diameter within the single crystal Y-123 matrix, as shown in our previous published work on experimental setting optimisation for YBCO characterisation (*11*).

4.2: SRIM/TRIM theoretical predictions of implantation depths and damage

SRIM (Stopping Ranges of Ions in Matter) and TRIM (TRajectories of Ions in Matter), as open access resources, have become common practice to predict the damage depths and calculate doses produced by ion implantation (*14*). For the present work, the full cascade model was used, with displacement energy of 30 eV and a density of 5.51 g/cm^3. These values were selected based on the work of Antonova *et al.* (*10*). Sources of errors can arise as SRIM assumes an amorphous target and relies on a Monte Carlo approach to predict binary collision approximations. Nevertheless, the predicted damage depth was between 800-900 nm, with peak damage around 300-500 nm. The output of the calculations is shown in Figure 1.
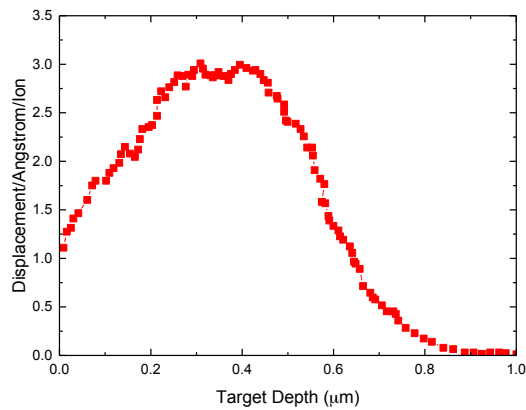

Figure 1: SRIM-Predicted implantation profile for the selected conditions (2MeV Xe$^+$ with a fluence of 1x10^{16} ions/cm^2).

4.3: Microstructural characterisation of the irradiated sample

The SRIM predicted damage depths were then confirmed by TEM. Figure 2 (a) shows an overview of the whole TEM sample, as a collage of TEM bright-field micrographs. The surface damage layer is shown to extend by ~900 nm into the sample. In bright-field the damaged layer has homogeneous contrast, which can be a sign of lack of crystallography (further confirmed in Figure 3). However, when imaged with HAADF-STEM (shown in Figure 2 (b)), Z-contrast now shows the local changes in composition where Y-211 particles used to be.
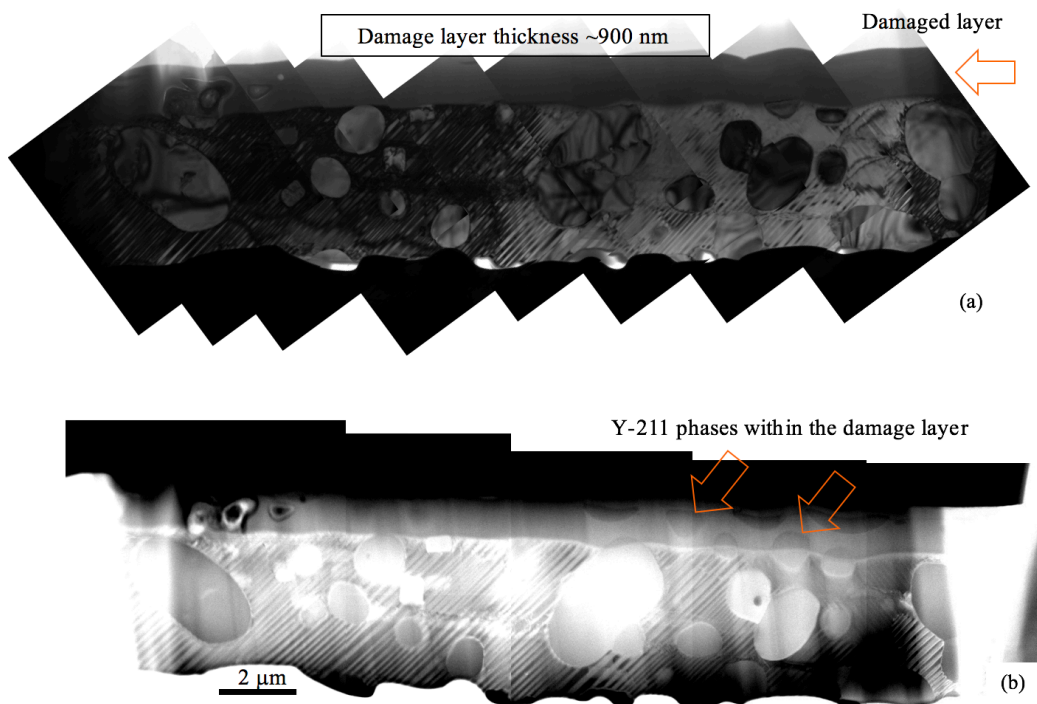
Figure 2: (a) TEM bright field micrograph of the whole sample, showing the damaged layer on the top surface, several Y-211 particles and the Y-123 matrix. (b) HAADF-STEM micrograph of the same region, taken at the same magnification. This time the improved Z-contrast allows the Y-211 particles in the damaged zone to be visible, despite being amorphous

The damaged layer was found to be fully amorphous, as proved through TEM diffraction in Figure 3. Figure 3 (b) shows a TEM bright-field micrograph indicating the regions from which selected area diffraction patterns were acquired, (a) shows an indexed diffraction pattern from the crystalline sub-surface region. Commercial TEM image simulation software JEMS was used to generate a theoretical diffraction pattern for Y-123 along the <111> zone axis which was overlayed and proved to match the experimentally acquired pattern in figure 3 (c). Finally, a diffraction pattern was acquired from the damaged surface region of the sample, which is shown in figure 3 (d) and shows a fully amorphous structure.
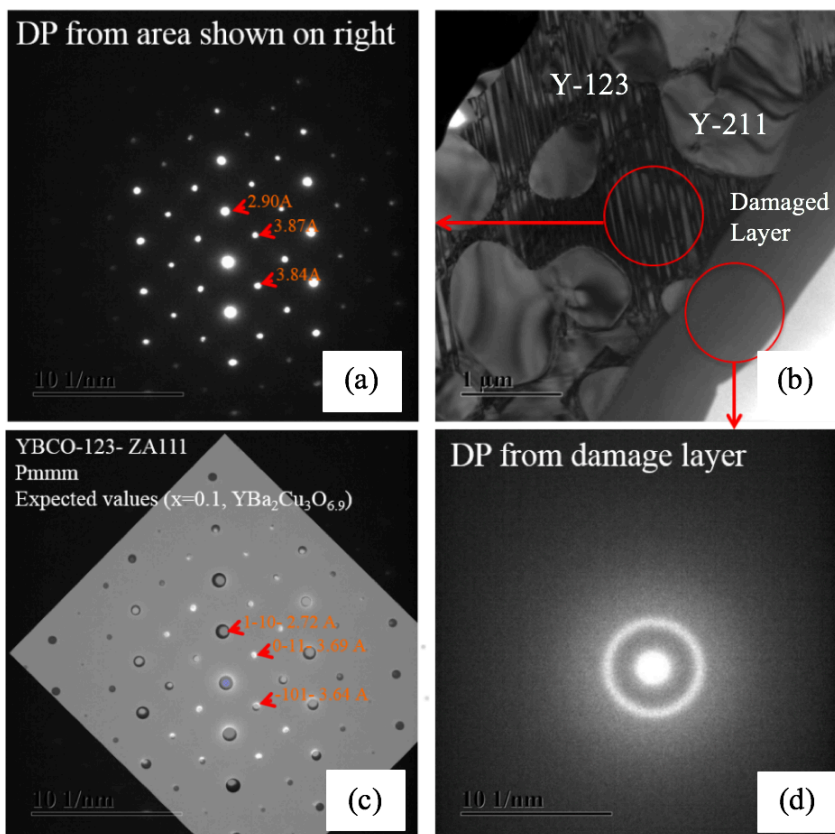

Figure 3: (a) diffraction pattern from crystalline region indicated by the arrow in the TEM bright field micrograph shown in (b), and with a theoretical pattern overlayed in (c). (d) shows the diffraction pattern from the fully amorphous damaged surface layer indicated by the arrow.

Some particles contained within the damage layer were however found to still show crystallographic (channelling) contrast in bright-field micrographs. One such example is shown in Figure 4 (a). When the selected area aperture was used to take a diffraction pattern it became evident that those particles were not fully amorphous. The diffraction pattern acquired, the region it was acquired from and the spots used for dark field image acquisition are shown in Figure 4 (b). Figure 4 (c) is the dark field image acquired. Figure 4 provides proof that not all the particles contained within the damaged zone are fully amorphous, and the ones that aren't have been shown by TEM-EDX to be made of barium cerate. Figure 5 shows the TEM-EDX maps acquired from one such particle. Cerium is only present in the sample due to the Ceria which were used as a Y-211 particle refiner during the TSMG process.
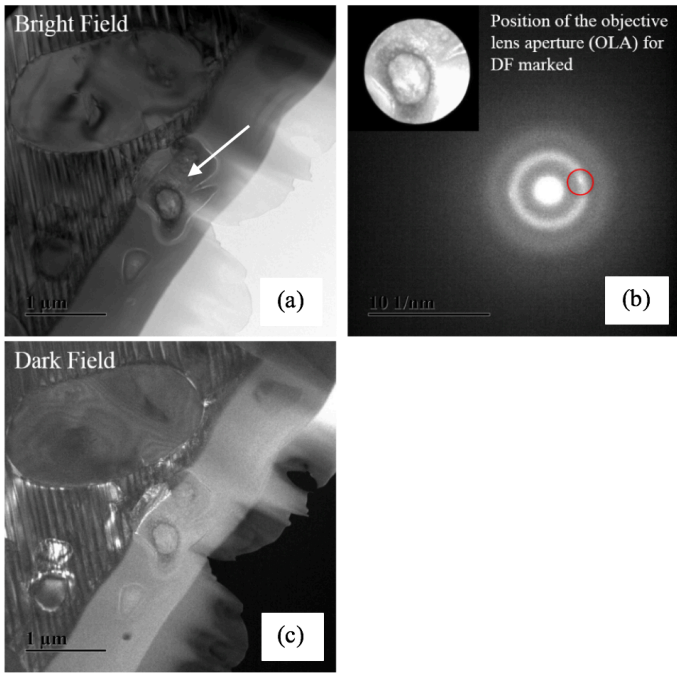
Figure 4: (a) Bright-field TEM micrograph showing a particle in the damaged layer which still exhibits crystallographic contrast, (b) diffraction pattern and the area it was taken from, showing a partially crystalline structure. (c) dark-field micrograph acquired using the diffracted spot indicated in (b).
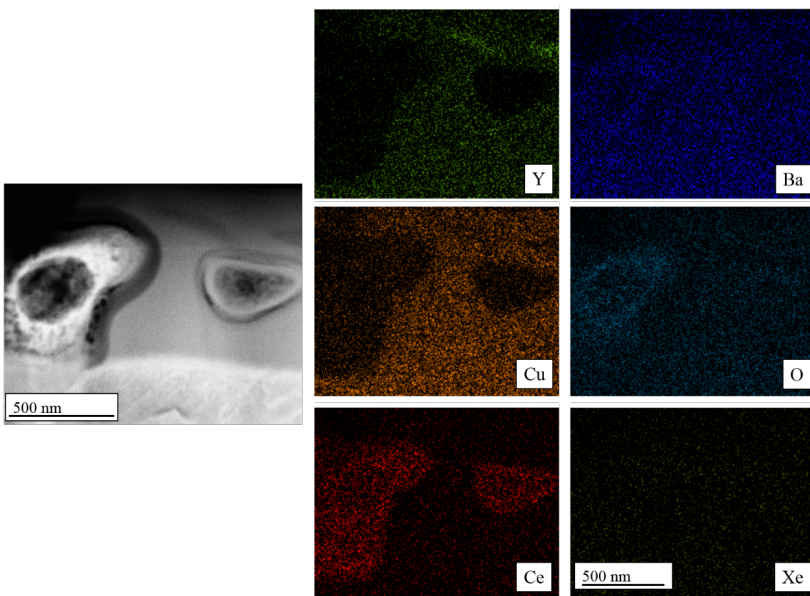

Figure 5: STEM-EDX map of the Cerium-rich particles which were partially crystalline in the damaged, amorphous layer.

While TEM studies are extremely useful in providing crystallographic information, atom probe tomography was used for accurate quantification of the local nano-scale sample stoichiometry. Since the full implanted region was 900 nm in length, it could not be analysed in its entirety within a single atom probe needle. The needles were made with the aim of placing the amorphous-to-crystalline interface within 300-400 nm from the apex, since that is a reasonable sample length which can be analysed. Figure 6 shows an APT reconstruction taken from the damaged layer after ion implantation. Figure 6 (a) shows a Y-211 particle and the interface with Y-123. The Xe content of the needle is shown in Figure 6 (b) and the associated mass spectrum is shown in Figure 6 (c). Xe is visible as a peak at 129 Da (only one isotope of Xe was used for ion implantation) and ~0.2at. % Xe was detected within the needle. Figure 6 (d) and (e) show the variations in chemical compositions along the z-axis of the needle. Due to the overall concentration of Xe and Ce being less than 1 at.% the signal-to-noise ratio is comparatively lower than for the other elements, as shown in Figure 6 (e). Nevertheless, the Xe composition profile is relatively uniform throughout the needle, and starts

to decrease after ~300 nm. Table 1 compares the measured chemical composition of the Y-123 phase before and after irradiation. No loss of oxygen was observed.

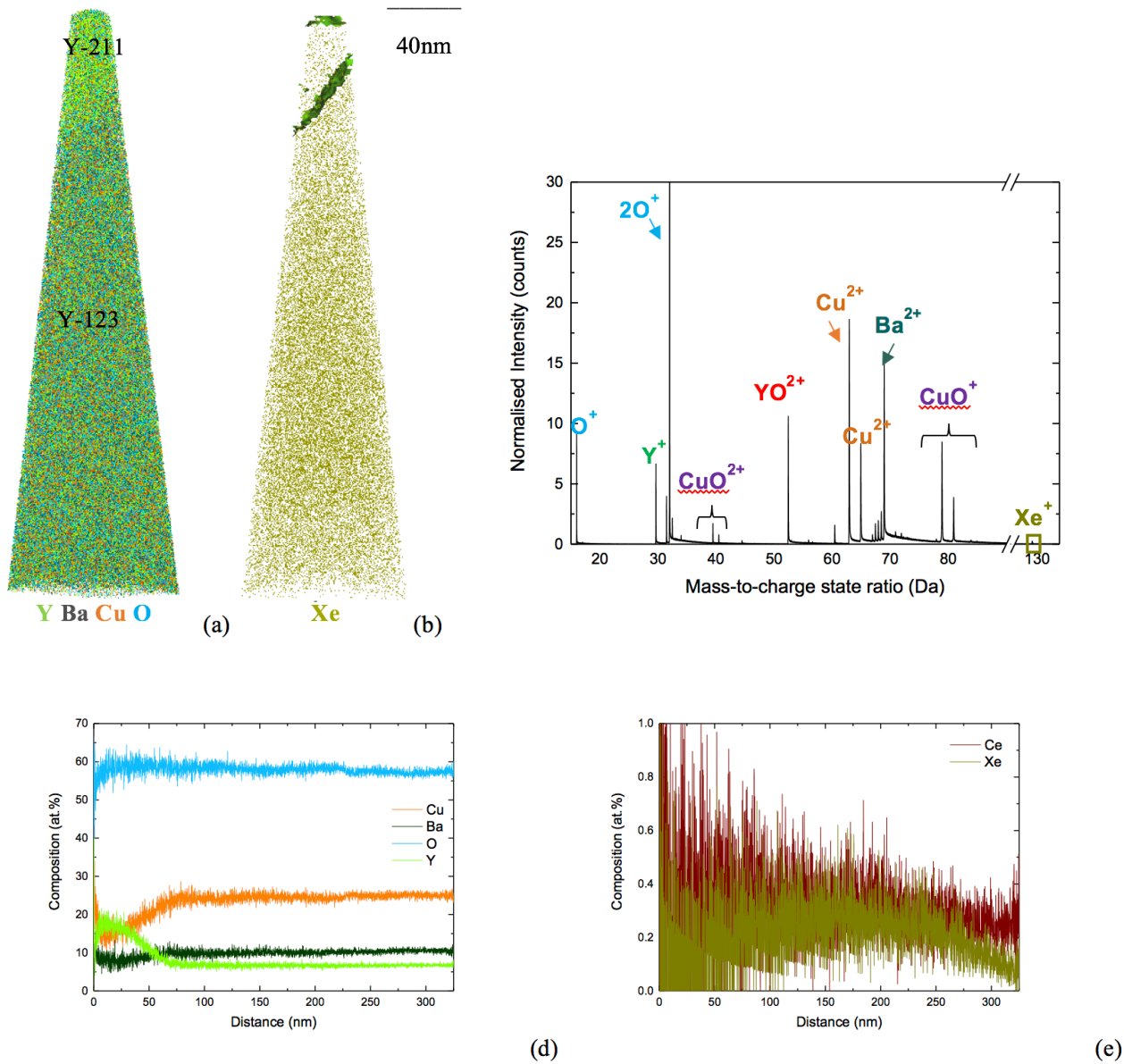Figure 6: (a) Atom probe reconstruction of the YBCO needle after Xe^+ implantation showing the Y. Ba. Cu and O ions, (b) showing the Xe ions. (c) mass spectrum of the implanted sample, (d) and (e) composition profiles along the length of the needle

Table 1: chemical compositions measurements before and after ion implantation.

At. %	Y	Ba	Cu	O	Ce	Xe
Unirradiated sample	7.4	11.8	24.6	55.9	0.2	0
Irradiated sample	7.5	10.1	25.3	57.3	0.3	0.2

4.4: Superconductivity

In order to assess the degradation in superconducting properties caused by the Xe^+ implantation, the critical current density as a function of applied magnetic field ($J_c(B_{app})$) was measured at 4.2 K, before and after implantation. A standard magnetic method was employed. The sample was cooled in a field value of -1.5 T, which was subsequently swept up to 7 T and back down to -1.5 T, measuring the induced magnetic moment of the sample (m) at 0.1 T intervals. Hysteresis loops are generated (as shown in Figure 7 (a)) due to circulating persistent currents in the sample. Employing Bean's model (15, 16) J_c is calculated from the hysteresis width (Δm) at any value of B_{app} by:

$$J_c(B_{app}) = \frac{3}{2\pi R^3 t} \Delta m(B_{app}),$$

where R is the sample's radius (1.5 mm), and t is the thickness of the superconducting film (nominally 1 μm). The resultant $J_c(B_{app})$ data are presented in Figure 7 (b) and summarized in Table 2. The secondary axis provides the corresponding wire I_c values that would be expected for the 4 mm wide tape.

As can be seen, the wire's current carrying ability at 4.2 K is reduced by a factor of 10. This can be attributed at least in part to a reduction in critical temperature (T_c) from 90 K to 80 K. To make a full assessment of the nature and extent of the damage inflicted by Xe^+ implantation would require detailed measurements to be made over a range of temperatures and field angles, along with corresponding measurements of the upper critical field B_{c2}. Nevertheless, the measurements made here demonstrate a catastrophic performance reduction that would almost certainly render the wire un-usable in fusion applications at these levels of damage.
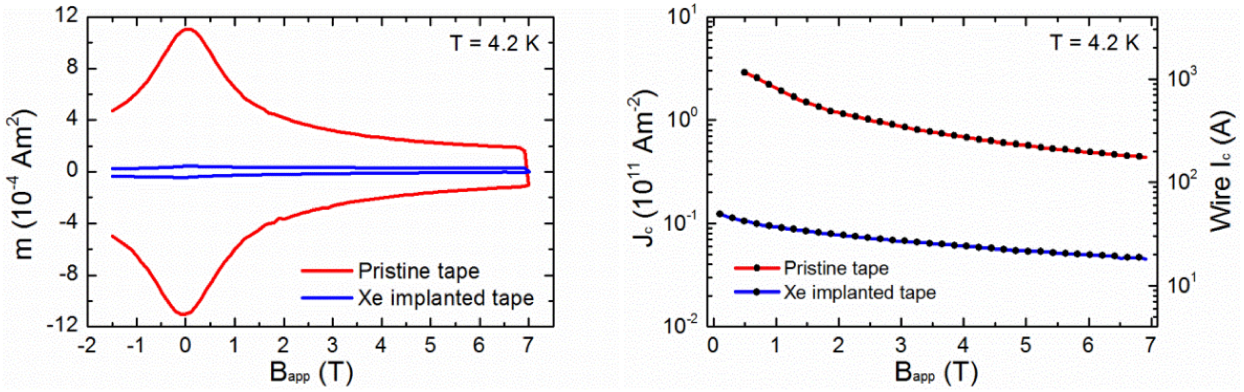

Fig 7: SQUID measurements on the tape before and after Xe implantation. (a) Magnetic hysteresis loops measured at 4.2 K for the 2G-HTS tape, before and after Xe implantation. The Cu and Ag overlayers were chemically removed from both samples prior to testing. (b) Critical current density as a function of magnetic field, calculated from the hysteresis widths of the data in (a), employing Bean's model. The secondary axis shows the equivalent critical current values expected for the 4 mm wide tape

Table 2: summary of the superconducting critical temperature at different fields and how it varied after ion implantation.

B[T]	T_c [K] Etched Tape	T_c [K] Xe Implanted Tape
0.01	90	80
2.00	83	66
4.00	78	55

4. Discussion:

Based on previous studies, Xe^+ implantation at a fluence exceeding 5×10^{12} ions/cm^2 is known to fully amorphise YBCO samples (10), though their study is not fully comparable due to the different irradiation energy. The present work performed at 1×10^{16} ions/cm^2 is consistent with those observations. Both the Y-123 and Y-211 phases were shown to be fully amorphous after ion implantation, however some ceria (fluorite) contained within the damage layer was not. The ceria is expected to be only present due to contamination introduced during the TSMG process. Ceria has been previously shown to exhibit outstanding phase stability under heavy ion irradiation, for example in the work by Edmondson et al., who implanted it with 3 MeV Au^+ ions at 3×10^{15} ions/cm^2 (17). The present observation of crystalline ceria within the

damaged zone can however have no influence on the alterations of superconducting properties of the fully amorphous matrix surrounding it.

The functional properties of amorphous YBCO are well known. It is being studied as it can be produced through deposition or sputtering techniques and has shown properties of interest for bolometric applications [Kreisler-2012]. Either when the material is fully amorphous or when oxygen depleted, YBCO is a known semiconductor [Degardin-2014]. Since oxygen depletion was shown to be negligible by APT in the present work, the 10-fold reduction in critical current density is expected to be the result of amorphisation.

Amorphisation kinetics and recovery mechanisms have not been previously studied in YBCO specifically, though numerous examples of models applied to other ceramics and perovskites can be found, as shown in the review by Weber [18]. Weber notes that the exact nature of amorphisation is not well defined for most ceramics, however various aspects of it can be described by the models developed. It is also important to note that ceramic amorphisation can occur homogeneously or heterogeneously, becomes increasingly difficult with increasing temperature and can only occur below a critical temperature [18].

Most perovskite ceramics are commonly described as amorphising heterogeneously, by one of several mechanisms, though that can depend on the irradiation conditions used. The most commonly suggested mechanisms, which were proposed for perovskite ceramics such as $ZrSiO_4$ and $SrTiO_3$, are either direct-impact (in-cascade) amorphisation of an individual collision cascade and the local defect accumulation as a result of cascade overlap [18]. An experimental study performed by HRTEM on Kr^+ irradiated YBCO at low fluence, ~10^{11} ions/cm^2, concludes that the defects they observe must be voids ~3-5 nm in diameter, though make no comment regarding their number density [19]. A theoretical study performed on YBCO predicted numerically through the Thermal Spike Model that when ion irradiated at a fluence of 10^{10}-10^{11} ions/cm^2, ion collision cascades may cause localised melting [19]. Their results estimate the characteristic size of the regions at ~50-70 nm, but variable depending on the ions used for implantation [20]. These findings suggest that amorphisation in YBCO may be heterogeneously nucleated and correlated mainly to the number of direct impacts coupled with defect accumulation due to cascade overlap.

Analytical models to describe this coupled effect were developed by Gibbons [21]. However, they neglect to account for materials recovery processes. Two main recovery processes reduce the amorphisation rate in ceramics: thermal and irradiation assisted recovery. Some perovskites such as $ZrSiO_4$ have been shown to exhibit mainly thermal-assisted recovery [18]. In order to attempt to model the findings, further studies are needed determining the amorphous fraction as a function of dose at several temperatures.

The concept of amorphisation becoming increasing harder with increasing temperature and only occurring below a specific critical temperature [18] leads to an intriguing possibility: could the damage be annealed out? If the stoichiometry is unaltered after ion implantation (which we proved to be the case), the crystal structure and therefore the superconductivity could be restored by a heat treatment. The component lifetime could be significantly extended, reducing the cost and environmental impact of radioactive waste disposal.

5. Conclusions:

The microstructure and electrical properties of YBCO superconducting tape and bulk samples were characterised before and after ion implantation. The present study proved that:

1. Atom probe tomography can be used to measure accurate chemical compositions (and in particular oxygen stoichiometry) in superconducting perovskite YBCO, though the interpretation of the results requires a detailed, systematic standardisation of the experimental and analytical conditions.
2. A Xe^+ ion implantation at a fluence of $1x10^{16}$ ions/cm^2 and energy of 2 MeV reduced the superconducting temperature by 10 K and cut the critical current density down to 1/10th of its former value.
3. The fluence and energy selected were predicted to damage the surface 800-900 nm of the samples, using SRIM software.

4. TEM characterisation revealed that the top 900 nm of the surface were fully amorphised after ion implantation. Of the original 1μm thick YBCO tape, only 1/10th remained crystalline.
5. Atom probe tomography did not detect alterations in local stoichiometry after ion implantation. No oxygen loss was detectable.
6. The amorphisation of the sample is expected to be the main contributing factor in the loss of superconducting properties.

References

1. A. Sykes *et al.*, Recent advances on the spherical tokamak route to fusion power. *IEEE Trans. Plasma*. **42**, 482–488 (2014).
2. E. I. Suvorova *et al.*, Structure analysis of the YBCO layer in Ag/YBCO/metal oxide buffer/Hastelloy composite tape before and after 107 MeV Kr17+ irradiation. *Acta Mater.* **75**, 71–79 (2014).
3. K. J. Leonard *et al.*, Irradiation Response of Next Generation High Temperature Superconductors for Fusion Energy Applications. *Fusion Sci. Technol.* **66**, 57–62 (2014).
4. A. A. Gapud *et al.*, Irradiation response of commercial, high-Tc superconducting tapes: Electromagnetic transport properties. *J. Nucl. Mater.* **462**, 108–113 (2015).
5. M. A. Kirk, Structure and flux pinning properties of irradiation defects in YBa_ {2} Cu_ {3} O_ {7-x}. *Cryogenics (Guildf)*. **33**, 235–242 (1993).
6. J. Barbour, E. Venturini, Irradiation effects in high temperature superconductors. *Nucl. Instruments ...* (1992) (available at http://www.sciencedirect.com/science/article/pii/0168583X92951006).
7. R. Weinstein, R. Sawh, J. Liu, D. Parks, Y. Ren, Threshold for creation of ionization pinning centers in YBCO by heavy ions. **360**, 743–746 (2001).
8. Y. Ren *et al.*, Isotropic short columnar pinning centers from fission fragment damage in bulk melt-textured YBCO, 9–10 (1997).
9. R. Biswal, D. Behera, D. Kanjilal, P. V. Satyam, N. C. Mishra, Evolution of superconducting and normal state properties of YBa2Cu3O7-y thick films under 200 MeV Ag ion irradiation. *Phys. C Supercond. its Appl.* **480**, 98–101 (2012).
10. L. K. Antonova *et al.*, Dependences of HTS tape critical parameters on fluences under irradiation with heavy ions and high energy electrons. *J. Surf. Investig. X-ray, Synchrotron Neutron Tech.* **5**, 484–491 (2011).
11. S. Pedrazzini *et al.*, Nano-scale stoichiometry analysis of a high temperature superconductor by atom probe tomography. *Ultramicroscopy*. **Under revi** (2016).
12. N. H. Babu *et al.*, Growth of large size Y1Ba2Cu3O7 single crystals using the top seeded melt growth process. *Supercond. Sci. Technol.* **25**, 75012 (2012).
13. G. D. Brittles, T. Mousavi, C. R. M. Grovenor, C. Aksoy, S. C. Speller, Persistent current joints between technological superconductors. *Supercond. Sci. Technol.* **28**, 93001 (2015).
14. J. F. Ziegler, J. P. Biersack, M. D. Ziegler.
15. C. P. Bean, Magnetisation of high-field superaconductors. *Rev. Mod. Phys.* **267** (1985).
16. C. P. Bean, Magnetization of hard superconductors. *Phys. Rev. Lett.* **8**, 250–253 (1962).
17. P. D. Edmondson, Y. Zhang, S. Moll, F. Namavar, W. J. Weber, Irradiation effects on microstructure change in nanocrystalline ceria − Phase , lattice stress , grain size and boundaries. *Acta Mater.* **60**,

5408–5416 (2012).

18. W. J. Weber, Models and mechanisms of irradiation-induced amorphization in ceramics. **167**, 98–106 (2000).

19. E. I. Suvorova *et al.*, Structure analysis of the YBCO layer in Ag/YBCO/metal oxide buffer/Hastelloy composite tape before and after 107 MeV Kr17+ irradiation. *Acta Mater.* **75**, 71–79 (2014).

20. A. Y. Didyk *et al.*, No Title. *Phys. solid state Condens. matter*. **5**, 739–744 (2013).

21. J. F. Gibbons, Ion Implantation in Semiconductors-Part Production and Annealing II : Damage. **6** (1972).